ARTICLES

Measuring Intramolecular Charge Transfer via Coherent Generation of THz Radiation

Matthew C. Beard, Gordon M. Turner, and Charles A. Schmuttenmaer*

Chemistry Department, Yale University, 225 Prospect St., P.O. Box 208107, New Haven, Connecticut 06520-8107

Received: September 21, 2001

We report the direct measurement of intramolecular electron transfer by detecting the electromagnetic (EM) waveform that is emitted during this process. It is detected in the time domain via free-space electro-optic sampling and then related to the dynamics of the charge-transfer event. Electromagnetic pulse generation from two systems, Betaine-30 in chloroform and DMANS in toluene, are studied to illustrate this technique. A finite-difference time-domain calculation with a time-dependent polarization is used to model the EM generation and propagation through the solution. This method is very general, since the movement of charge itself generates the EM waveform, and is sensitive to charge transfer occurring on a 0.1−10 ps time scale.

Introduction

Charge transfer and photoinduced charge transfer are ubiquitous phenomena. Photosynthesis, redox chemistry, corrosion, photography, xerography, respiration, and many other fundamental processes all rely on charge transfer. Because of this wide interest, a variety of experimental techniques has been developed over the years to study charge transfer dynamics. These techniques typically measure the charge-transfer event indirectly, for example, by monitoring the transient absorption or emission of the charge donor or acceptor.[1] In this work, we introduce a method that can monitor a charge transfer event directly without regard to the nature of the acceptor or donor groups. This new method is based on monitoring the electromagnetic (EM) waveform emitted by the motion of the charge.

Ever since James Clerk Maxwell wrote down his famous equations and Heinrich Hertz verified them experimentally, it has been well-known that any accelerating charge generates EM radiation.[2,3] Since charge transfer reactions involve movement of charge, they too generate EM transients. The detailed temporal form of the emitted waveform is directly linked to the underlying pulse generation dynamics. We employ the well-known technique of free space electro-optic sampling (FSEOS) to measure the emitted field amplitude with subpicosecond temporal resolution.[4−6]

To generate a pulse, the fields emitted by all of the individual molecules must add together constructively. For this to occur, there are two fundamental requirements; the molecules must be oriented, and they must be coherently excited. If the orientation is only about one axis, then a third requirement is that the charge transfer must induce a change in polarization along this orientation axis. For this study, we fulfill these requirements by partially orienting dipolar molecules in a static electric field prior to coherent photoexcitation.

We obtain two important pieces of information from this measurement. First, the polarity of the emitted field directly reveals the direction of the charge transfer. Second, the temporal form of the emitted field provides dynamical information. We illustrate this technique by comparing the EM pulse generated from two different dye molecules shown in Figure 1. The first is Betaine-30 [2,6-diphenyl-4-(2,4,6-triphenylpyridinio)-phenolate], or Reichardt's dye, dissolved in chloroform. Its dipole moment decreases and changes sign upon photoexcitation, and it has a very short excited-state lifetime, on the order of a picosecond.[7,8] The other molecule investigated is DMANS (4-(dimethylamino)-4′-nitrostilbene) dissolved in toluene. Its dipole moment increases upon photoexcitation, and its excited-state lifetime is on the order of 10 ns.[9,8]

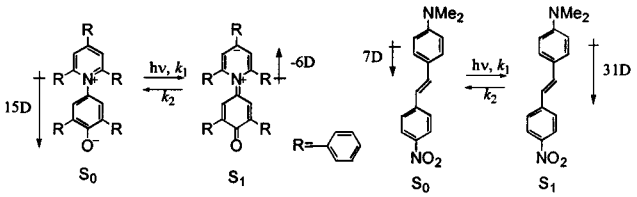

Figure 1. The ground, S_0, and first excited states, S_1, of Betaine-30 (left) and DMANS (right) and their respective dipole moments.

Two techniques closely related to this method are THz generation from biased semiconductors and the transient dc photocurrent (TDP) technique. THz generation from biased semiconductors utilizes the EM pulse generated to probe ultrafast carrier dynamics in semiconductors[10,11] and quantum wells.[12,13] The TDP technique measures the change in polarization of a solution after photoexcitation.[9] A displacement current is generated when the photoexcited molecules reorient in a static field. The TDP technique can measure ground and excited-state dipole moments as well as long-lived excited-state lifetimes. However, it is limited in temporal resolution, and cannot measure the earliest charge-transfer dynamics. Our new technique complements the TDP technique in that both methods measure the change in polarization after photoexcitation, but on very different time scales.

A related technique is that of coherent infrared emission (CIE) interferometry.[14] In CIE, vibrations are coherently excited via

10.1021/jp013603l CCC: $22.00
Published on Web 01/17/2002

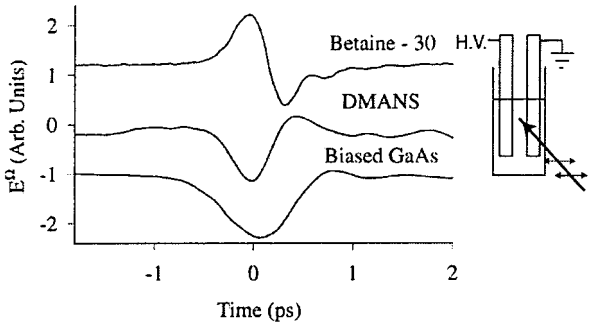

Figure 2. Electric fields generated via charge transfer in DMANS and Betaine-30 compared to that generated from photoexcitation of biased GaAs. The applied field is in the same direction in each case. The experimental configuration is shown to the right.

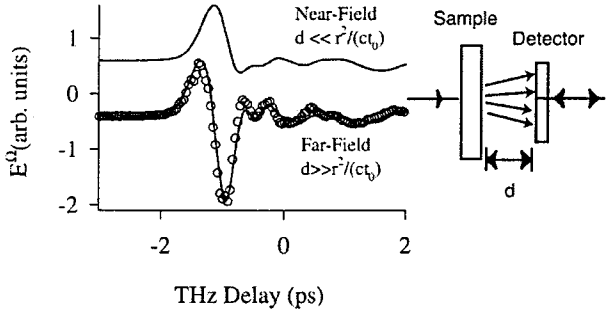

Figure 3. THz generation is produced from ZnTe via optical rectification to illustrate near- vs far-field regimes. The open circles are the first derivative of the near-field signal while the lines are the measured near-field and far-field signals. The detector configuration is shown to the right.

an ultrafast electronic excitation and emit an EM field that is detected interferometrically. Only vibrations that are coupled to the electronic excitation will contribute to the emitted field, and in that sense, it is similar to a stimulated resonance Raman experiment. Our technique is similar to stimulated resonance Raman in that a low-frequency oscillation coupled to an electronic transition emits a field. In our case, it is the charge transfer; in the case of CIE, it is the intramolecular vibrations. Our technique also is sensitive to any intramolecular vibrations that are coupled to our excitation pulse; however, our bandwidth limits us to far-infrared frequencies. Furthermore, these oscillations, if present, cause a change in dipole that is orders of magnitude smaller than that caused by the charge transfer and are below our current signal-to-noise ratio.

Experimental Section

A regeneratively amplified Ti−Sapphire laser produces 100 fs, 800 nm pulses at 1 kHz with 1 W average power and are split into two beams, one to photoexcite the sample and the other to detect the EM transient. Detection of the EM transient occurs via FSEOS in a 0.5 mm thick ⟨110⟩ ZnTe crystal.[6,15] Approximately 2.3 mJ/cm^2 at 800 nm was used to excite the Betaine-30 solution. DMANS was excited at 400 nm with 1 mJ/cm^2. The excitation pulse beamwaist was about 2.5 mm diameter at the cuvette.

The dye solution is held in a 1 mm path length quartz cuvette with a pair of rectangular metal strips inserted as electrodes (see Figure 2). High voltage (0.5−3 kV) pulses are used rather than a static field to avoid unnecessary heating of the solution. However, the high voltage pulses are ∼100 μs in duration and are considered static with respect to the 100 fs laser excitation pulse. The electrodes are typically 3−4 mm apart, resulting in electric fields of 1.5−10 kV/cm. Dye concentrations are between 3.0×10^{-3} and 6.0×10^{-3} mol/L.

To reconstruct the charge transfer dynamics, great care must be taken when collecting the signal to avoid distortion of the generated waveform. The detector is placed adjacent to the sample as shown in Figure 3, and no focusing or directing optics are used. Collecting the data in this manner allows us to obtain the true underlying dynamics, but at the cost of a lower signal-to-noise ratio. Ideally, the signal would be collected in the near-field regime, which would allow the pulse shape to be measured directly. However, the relatively small excitation spot size and the fact that the cuvette walls are 1-mm thick prevent us from placing the detector close enough to the photoexcited medium to be in the near-field. Therefore, the signal is collected in the far-field regime. The far-field is defined[16] as $d >> r^2/ct_0$, where d is the distance of the detector from the sample, r is the transverse radius of the visible pump beam, and t_0 is the full width at half-maximum of the transient. For these studies, $r^2/ct_0 \approx 1$ cm, and we ensure that we are in the far-field by increasing d until the pulse shape no longer changes with increasing distance, at which point d is about 3 cm. By collecting the signal in this manner we avoid difficulties of astigmatism, Guoy phase shift[16−18] and other diffraction-induced pulse distortions that occur with large bandwidth pulses.

The far-field pulse shape is related to the near-field pulse by a time derivative.[16,19] We have verified this relationship for our apparatus by using ZnTe as both the generator and detector. We can expand the beam waist when using the highly efficient ZnTe generator, such that the near-field regime is obtainable. A comparison of the near- and far-field signals is shown in Figure 3.

Results and Discussion

Electromagnetic pulse generation from biased GaAs is used to calibrate the polarity of the measured signal. Figure 2 displays the EM transients generated from biased GaAs, Betaine-30, and DMANS. In each case, the applied field is in the same direction. Photoexcitation of biased GaAs produces electrons that are accelerated toward the positive electrode; this results in a generated field with *negative* polarity (a field is defined by its effect on a positive point test charge). An *increase* in dipole moment along the applied field axis upon photoexcitation will result in a signal with the same polarity as GaAs, as is obtained from DMANS. Electromagnetic pulse generation from Betaine-30, on the other hand, exhibits a *positive* polarity because its dipole moment *decreases* upon photoexcitation.

Additionally, Betaine-30 may be excited with 400 nm light into a higher electronic state whose dipole moment does not change from the ground state—it is a local excitation of the phenolate group.[7] This state rapidly undergoes charge transfer to the S_1 state (∼200 fs). Therefore, photoexcitation at 400 nm should also generate an EM pulse, and it should have the same polarity as 800 nm excitation, and we have verified that it does.

The generated field amplitude was monitored as a function of excitation intensity, polarization, and static field amplitude, as shown in Figure 4, to fully characterize the technique. The generated field amplitude varies linearly with the applied field amplitude, and linearly with the visible intensity; therefore, it has a quadratic dependence on the visible pulse amplitude. Thus, $E^{\Omega} \propto E^0 E^{\omega} E^{\omega}$, where E^{Ω} is the generated THz field amplitude, E^0 is the local static field amplitude, which is different from the applied static field due to the solvent permittivity, and E^{ω} is the visible field amplitude. These dependencies indicate a third-order nonlinear interaction. We have verified that the pulse

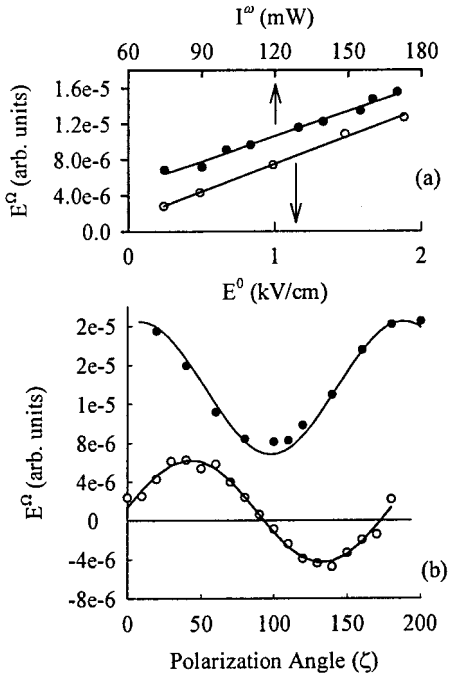

Figure 4. Dependence of the generated signal amplitude with (a) visible intensity (filled circles) and static field amplitude (open circles) and (b) visible polarization angle, detecting the *X* component (filled circles) and *Y* component (open circles) of the generated pulse amplitude.

shape does not change with the applied field or with the visible intensity, only the magnitude changes.

While this work is carried out in the time-domain, it is conventional to introduce a frequency-domain third-order susceptibility tensor and relate it to the measured signal. For these measurements, the appropriate susceptibility is given by the following standard notation[20] $\chi^{(3)}_{ijkl}(-\Omega; \omega, -\omega, 0)$, where Ω refers to the emitted frequency, ω to the visible frequency, and 0 denotes the static field. Note that Ω is nonzero only because the short visible pulses have bandwidth of a few hundred wavenumbers centered at ω. We refer to this new technique as CTIEG (charge-transfer induced electromagnetic pulse generation). The susceptibility tensor describes the flow of energy among the different propagating EM fields in a given medium and describes the matter-field interactions, which are of fundamental interest. The third-order time-domain response function, $R^{(3)}_{ijkl}(t_1, t_2, t_3)$ is related to the frequency domain susceptibility through a triple inverse Fourier transform[20]

$$R^{(3)}_{ijkl}(t_1, t_2, t_3) = \mathrm{FT}^{-1}\{\chi^{(3)}_{ijkl}(-\Omega; \omega, -\omega, 0)\} \qquad (1)$$

The indices of the third-order nonlinear susceptibility tensor, $\chi^{(3)}_{ijkl}$, refer to the lab-fixed Cartesian directions *X*, *Y*, and *Z*. The polarization of the emitted pulse is indicated with *i*, the visible laser polarization is represented in *j* and *k*, and the static field direction is *l*. The pulse propagates in the *Z* direction. The static field direction is fixed for our studies and defines the *X* direction, and thus, $l = X$. In general, the emitted field is linearly polarized at an angle ϕ relative to the *X* direction and depends on the angle of the visible polarization (ζ) with respect to the *X* direction.

For isotropic media, there are only three independent tensor elements of $\chi^{(3)}_{ijkl}$, and they are related by[20]

$$\chi^{(3)}_{XXXX} = \chi^{(3)}_{XYYX} + \chi^{(3)}_{YXYX} + \chi^{(3)}_{YYXX} \qquad (2)$$

If we assume Kleinman symmetry,[21,20] then $\chi^{(3)}_{XYYX} = \chi^{(3)}_{YYXX} = \chi^{(3)}_{YXYX}$ and $\chi^{(3)}_{XXXX} = 3\chi^{(3)}_{XYYX}$. From these relationships, we can determine the amplitude and direction of the induced third-order polarization, $P^{(3)}$, in terms of $\chi^{(3)}_{XYYX}$. The *X* and *Y* components of $P^{(3)}$ are

$$P^{(3)}_X(\zeta) = \chi^{(3)}_{XYYX} I^{\omega}_{jk} E^0_X(3\cos^2\zeta + \sin^2\zeta), \quad \text{and}$$

$$P^{(3)}_Y(\zeta) = \chi^{(3)}_{XYYX} I^{\omega}_{jk} E^0_X(2\sin\zeta\cos\zeta) \qquad (3)$$

where I^{ω}_{jk} is the intensity of the visible pulse with polarization angle ζ relative to the *X* direction. The visible polarization vector, $\hat{e}_{jk}$, is given by $\hat{e}_{jk} = \hat{e}_X \cos\zeta + \hat{e}_Y \sin\zeta$. The emitted polarization is at an angle ϕ with respect to the static field and is obtained from the *X* and *Y* components

$$\mathbf{P}^{(3)}_{\phi} = P^{(3)}_X \hat{X} + P^{(3)}_Y \hat{Y} \qquad (4)$$

where $\phi = \arctan[(2\cos\zeta\sin\zeta)/(3\cos^2\zeta + \sin^2\zeta)]$. The *X* and *Y* components of the emitted field are shown in Figure 4b and compared to eq 3 (shown with a solid line) and verify that Kleinman symmetry is valid for this type of experiment. This is because the change in dipole that generates the signal is along the ground-state dipole axis.

The tensorial nature of the third-order susceptibility reflects the induced anisotropy caused by the visible and static fields. The interaction of the static electric field with a dipolar molecule in solution results in a fractional orientation of the molecules along the field direction, which provides the underlying physical basis for this method. This fractional orientation can be calculated by considering the interaction energy of a dipole with an applied field, $\boldsymbol{\mu}\cdot\mathbf{E}^{\circ}$ in comparison to $k_B T$, where k_B is Boltzmann's constant and *T* is the temperature in Kelvin. It is expressed as a function of angle (θ) between the applied field and molecular dipole moment by[9,22]

$$f(\theta) = \frac{e^{-V/k_B T}}{\int_0^{2\pi} e^{-V/k_B T}\, d\theta} \approx \frac{1}{2\pi}\left(1 + \frac{\mu E^0 \cos\theta}{k_B T}\right) \qquad (5)$$

where the interaction potential, *V*, is given by $V = -\mu E^0 \cos\theta$. Terms resulting from polarizability anisotropy have been neglected. Given the inherent azimuthal symmetry, we work in polar coordinates. Thus, interaction with the static field results in a linear combination of an isotropic and a $\cos\theta$ distribution. The visible pulse introduces a $\cos^2(\theta - \zeta)$ distribution of excited molecules due to projection of the transition dipole moment onto its polarization. An additional factor of $\cos(\theta - \phi)$ results from a projection of the emitted polarization onto an axis at angle ϕ. Thus, the emitted amplitude at a given polarization angle ϕ varies as a function of visible polarization angle (ζ) as

$$E_{\phi}^{\Omega}(\zeta) \propto \int_0^{2\pi} \cos(\theta)\cos^2(\theta - \zeta)\cos(\theta - \phi)\, d\theta = A(\zeta,\phi) \qquad (6)$$

where the integral evaluates to

$$A(\zeta,\phi) = \frac{\pi}{4}[\cos\phi\,(3\cos^2\zeta + \sin^2\zeta) + 2\sin\phi\cos\zeta\sin\zeta] \qquad (7)$$

It can easily be verified that eq 7 is equivalent to the angular dependence of $P^{(3)}_{\phi}$ in eq 4, and the two formalisms are complementary.

Modeling the Data

If propagation effects of the fields through the solvent can be neglected, then the emitted amplitude in the far-field regime

is equal to the second derivative of the time-dependent polarization,[23] $E_i^{\Omega} = \partial^2 P_i/\partial t^2$. However, nonnegligible propagation effects such as group velocity mismatch between the visible and generated EM pulses, absorption of the visible pulse by the solution, and dispersion of the generated pulse by the solvent must be accounted for in order to correctly obtain the charge transfer dynamics. We do so by numerically solving Maxwell's equations in the time domain[24] coupled to a phenomenological model for the time-dependent polarization. We then perform a nonlinear least-squares fit of the model to the data to obtain the charge-transfer dynamics.

For a transverse electric field and no free currents, the wave equation in one dimension is[20]

$$\frac{\partial^2 E(z,t)}{\partial z^2} - \frac{1}{c^2}\frac{\partial^2 E(z,t)}{\partial t^2} = \mu_0 \frac{\partial^2 P(z,t)}{\partial t^2} \tag{8}$$

where c is the speed of light in a vacuum, $E(z,t)$ is the electric field at position z and time t, and $P(z,t)$ is the induced polarization. We separate the polarization P into linear and nonlinear contributions. Only the third-order nonlinear term contributes to the generated pulse, whereas the linear term describes dispersion and attenuation of the generated signal as it propagates through the solvent. Therefore, eq 8 becomes

$$\frac{\partial^2 E^{\Omega}(z,t)}{\partial z^2} - \frac{1}{c^2}\frac{\partial^2}{\partial t^2}\int_0^t R^{(1)}(t-t')E^{\Omega}(t',z)\,\mathrm{d}t' = \mu_0 \frac{\partial^2 P^{(3)}(z,t)}{\partial t^2} \tag{9}$$

for the generated field E^{Ω} where $R^{(1)}(t)$ is the linear response of the solvent to the generated field. Equation 9 describes the simultaneous generation and propagation of the EM transient through the dye solution. The linear term is known from measurement of static THz pulse propagation through the solution without excitation, and only the third-order polarization is needed to close eq 9.

In the most general terms, the third-order nonlinear polarization (in suffix notation) is given by[20]

$$P_i^{(3)}(t,z) = \epsilon_0 \int_{-\infty}^{\infty}\mathrm{d}t_1 \int_{-\infty}^{\infty}\mathrm{d}t_2 \int_{-\infty}^{\infty}\mathrm{d}t_3\, R_{ijkl}^{(3)}(t-t_1, t-t_2, t-t_3) E_j(t_1,z)E_k(t_2,z)E_l(t_3,z) \tag{10}$$

where $R_{ijkl}^{(3)}$ is the third-order time-domain response function, E_j, E_k, and E_l are given by $E_m(z,t) = \hat{e}_m E^{\omega}(z,t)e^{-i\omega t} + \hat{e}_m^* E^{-\omega}(z,t)e^{i\omega t} + \hat{e}_X E^{\circ}$, where $E^{\omega}(z,t)$ is the visible field envelope (taken to be a Gaussian function), and $\hat{e}_m$ describes its polarization vector. Only linearly polarized light is used; therefore, $\hat{e}_m = \hat{e}_m^*$. We retain only those terms that contain the product of the three fields, $E^{\omega}E^{-\omega}E^{\circ}$. Since E° is time-independent, we need not integrate over t_3,[20] which yields $R_{ijkl}^{(3)}(t-t_1, t-t_2, t-t_3) = R_{ijkX}^{(3)}(t-t_1, t-t_2)\delta(t-t_3)$. Since electronic dephasing is fast compared to the visible envelope we let $t_2 = t_1 = t'$. The simultaneous propagation of the visible pulse is accounted for by including the absorption coefficient α, and its group velocity v_g. We arrive at the following equation for the induced polarization:

$$P_i^{(3)}(z,t) = \epsilon_0 \int_0^t \mathrm{d}t'\, I_{jk}^{\omega}(z,t''-t')R_{ijk,X}(t') \tag{11}$$

where $I_{ij}^{\omega}(z,t) = E^{\omega}(z,t)E^{-\omega}(z,t)\hat{e}_{jk}\exp(-\alpha z)$, $R_{ijkX}^{(3)}(t') = 0$ when $t'' < 0$ and $t'' = t - (z/v_g)$, the index i defines the angle ϕ from the X direction, and the pair of j and k define angle ζ. The response function $R_{ijkX}^{(3)}(t)$ can now be viewed as the impulse response function to a delta function excitation pulse.

To model $R_{ijkX}^{(3)}(t)$, consider a delta function excitation pulse of a single dye molecule at $z = 0$ and $t' = 0$. The pulse induces an electron transfer with rate k_{ET} and subsequent back electron transfer with rate k_{BET}, and the contribution to the change in polarization is given by

$$\Delta p(t) = \frac{k_{ET}}{(k_{BET} - k_{ET})}[\exp(-k_{ET}t) - \exp(-k_{BET}t)]\Delta'\mu \tag{12}$$

where $\Delta'\mu$ is the change in dipole moment along the ground-state dipole. We average the contributions from individual molecules over an anisotropic distribution that is created by the visible and static fields. Since reorientation of the excited molecules occurs on a longer time scale than that of these measurements, the orientational average is given by

$$\langle\Delta'\mu\rangle = \mu'_e \int_o^{2\pi} f(\theta)\cos^2(\theta-\zeta)\cos(\theta-\phi)\,\mathrm{d}\theta = \frac{E^0}{8k_BT}A(\zeta,\phi)(\mu'_e - \mu_g)\mu_g \tag{13}$$

where μ_g is the ground-state dipole moment and μ'_e is the projection of the excited-state dipole moment along the ground-state dipole moment. Thus, the change in polarization is obtained by replacing $\Delta'\mu$ with $\langle\Delta'\mu\rangle$ in eq 12.

The solvent molecules also affect the measured change in polarization, so we must account for their reaction field. The electrostatic potential of a dipole in solution is modified from its value in a vacuum by the reaction potential of the polarized surrounding dielectric medium. Upon photoexcitation, the electrostatic potential changes abruptly, and therefore, a repolarization of the solvent occurs. If the change in dipole is fast compared to the solvent motions, then the measured change in polarization will reflect this solvent repolarization. We describe the solvent response as an impulse response function to a delta function change in the solute charge configuration. We treat the solvent response as a single exponential, and the combined solvent−solute polarization p_s response to an impulse excitation pulse is given by

$$p_s(t) = \int_0^t \mathrm{d}t'\,\Delta p(t')\Phi(t-t') \tag{14}$$

where $\Phi(t) = \exp(-k_s t)$ represents the response of the solvent with rate constant k_s. If $k_s \ll k_{ET}$, the rise of the signal will be governed by the polarization of the solvent.

The solute−solvent polarization is in fact the third-order response function required in eq 11. That is $R_{ijkX}(t) = p_s(t)$, and the third-order polarization is obtained from

$$P_i^{(3)}(t,z) = \epsilon_0\int_0^t \mathrm{d}t'\, I_{jk}^{\omega}(z,t''-t')R_{ijkX}^{(3)}(t') = \epsilon_0\int_0^t \mathrm{d}t'\, I_{jk}^{\omega}(z,t''-t')\int_0^{t'}\mathrm{d}t'''\,\Delta p(t''')\Phi(t'-t''') \tag{15}$$

The finite difference time domain (FDTD) method[24] is used to numerically solve eq 9 coupled with eq 15. The advantage of using the FDTD method is that the slowly varying envelope approximation and rotating wave approximation are not assumed. While these approximations are valid for the visible pulse, they are not applicable for the generated EM pulse. Furthermore, the FDTD method completely accounts for the generation term as well as the dispersive term, and group

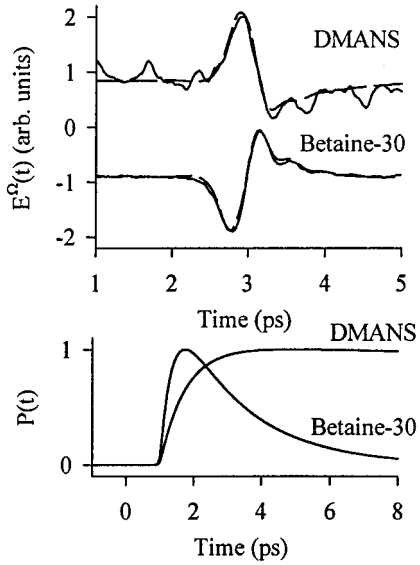

Figure 5. Results of the nonlinear least-squares fit of the model to the data. The time-dependent polarization is shown below. The time constants are given in Table 1.

TABLE 1: Optimized Parameters Resulting from Nonlinear Least Squares Fits for Betaine-30 in Chloroform and DMANS in Toluene[a]

	Δw (fs)	k_s (ps^{-1})	τ_s (fs)	k_{ET} (ps^{-1})	k_{BET} (ps^{-1})	τ_{BET} (ps)
Betaine-30	150[b]	2.86	350	>100[b]	0.53	1.9
DMANS	150[b]	1.37	730	>100[b]	<0.01[b]	>100[b]

[a] The corresponding time constants are included for convenience. The Gaussian width is given by Δw. [b] Values held fixed during the fit.

velocity mismatch is automatically included in the simulation. The FDTD calculation provides the generated field in the near-field regime, and a near-field to far-field transformation is performed by taking the first derivative of the calculated field. The ZnTe detector further distorts the measured signal, and a numerical propagation through the detector is included in the simulations.[5,25] A nonlinear least-squares fit is performed in order to extract the best-fit values of the forward and back electron-transfer rates. The results of the fit are shown in Figure 5, and the rate constants are provided in Table 1.

ET Rate Constants

The initial photoexcitation of Betaine-30 and DMANS is instantaneous; that is, it is purely electronic and occurs faster than the response of the solvent, $k_s \ll k_{ET}$. The rise time of our signal is governed by the response of the solvent to a new charge distribution. In our fits, k_{ET} is held fixed at a large value, on the order of 1 fs^{-1} (10^{15} s^{-1}), corresponding to a 1 fs electron transfer time constant. We find solvent response times of roughly 350 and 730 fs for Betaine-30 chloroform and DMANS in toluene, respectively.

The solvent response times determined here are on the same time scale as those determined from time-resolved fluorescence Stokes shift (TRSS) and optical heterodyne detected Raman-induced Kerr effect spectroscopy (OHD-RIKES) experiments.[26] Those experiments typically find the response to be either multiexponential or having a fast Gaussian component, followed by a biexponential decay. There is usually a contribution with a time constant of several hundred femtoseconds. Recently, Castner and Maroncelli have provided power law relations to compare TRSS, OHD-RIKES, and dielectric relaxation data; testing the assumption that single-particle reorientational motion is the underlying basis for each type of measurement. They find that TRSS and dielectric relaxation data are satisfactorily related to each other, but not to OHD-RIKES results.

It is important to note that the solvent response we measure is not simply the time-domain representation of its IR spectrum. For example, the dipole−dipole time correlation function for chloroform is essentially single exponential with a 4 ps time constant.[27] Furthermore, any distortion of the pulse as it travels through the solvent is explicitly accounted for in the FDTD simulation. One possible reason that the measured solvent response is different from the bulk solvent response (based on its IR spectrum) is that the molecules interact with the solute and are partially oriented around it. Thus, as the field is emanating from the dye molecule, it encounters a medium that differs from the bulk solvent. Another possible reason stems from the fact that the solvent has a wave vector dependent response. The response of the first solvation shell will correspond to a nonzero wave vector ($k > 0$), whereas when a pulse travels through a medium, it probes the dynamics having wave vector of zero ($k = 0$).

We can compare the extracted back electron-transfer time with those of other measurements. Our value of 1.9 ps for the back electron-transfer time corresponds well with previous work on Betaine-30 where values of 1.4 ps in acetonitrile, 1.2 ps in acetone and 2.1 ps in toluene were reported.[7]

Conclusions

We have presented a new technique of measuring ultrafast charge-transfer dynamics in solution that occur on a time scale of 0.1−10 ps. This technique is independent of the properties of the acceptor and donor groups because it is the motion of the charge that generates the signal. The technique is generalizable to any charge-transfer event that occurs rapidly, if an appropriate orientation of the charge-transfer event can be arranged. That is, this technique is not limited to dipolar molecules that can be oriented by a static field. For example, self-assembled-layered structures could provide the desired orientation. This technique is well suited to answer long-standing questions with regard to charge-transfer events where conventional techniques are ambiguous, such as the primary charge separation event in photosynthetic systems.

Acknowledgment. Support from a National Science Foundation CAREER award (CHE-9703432) is gratefully acknowledged.

References and Notes

(1) Barbara, P. F.; Meyer, T. J.; Ratner, M. A. *J. Phys. Chem.* **1996**, *100*, 13148−13168.

(2) Jenkins, F. A.; White, H. E. *Fundamentals of Physical Optics*, 1st ed.; McGraw-Hill: New York, 1937.

(3) Jackson, J. D. *Classical Electrodynamics*; John Wiley & Sons: New York, 1962.

(4) Lu, Z. G.; Campbell, P.; Zhang, X. C. *Appl. Phys. Lett.* **1997**, *71*, 593−595.

(5) Beard, M. C.; Turner, G. M.; Schmuttenmaer, C. A. *Phys. Rev. B* **2000**, *62*, 15764−15777.

(6) Wu, Q.; Zhang, X. C. *Appl. Phys. Lett.* **1995**, *67*, 3523−3525.

(7) Levinger, N. E.; Johnson, A. E.; Walker, G. C.; Barbara, P. F. *Chem. Phys. Lett.* **1992**, *196*, 159−165.

(8) Liptay, W.; Dumbache. B.; Weisenbe. H. *Z. Naturforsch., A: Phys. Sci.* **1968**, *23*, 1601.

(9) Smirnov, S. N.; Braun, C. L. *Rev. Sci. Instrum.* **1998**, *69*, 2875−2887.

(10) Leitenstorfer, A.; Hunsche, S.; Shah, J.; Nuss, M. C.; Knox, W. H. *Phys. B* **1999**, *272*, 348−352.
(11) Hu, B. B.; Desouza, E. A.; Knox, W. H.; Cunningham, J. E.; Nuss, M. C.; Kuznetsov, A. V.; Chuang, S. L. *Phys. Rev. Lett.* **1995**, *74*, 1689−1692.
(12) Luo, M. S. C.; Chuang, S. L.; Planken, P. C. M.; Brener, I.; Roskos, H. G.; Nuss, M. C. *IEEE J. Quantum Electron.* **1994**, *30*, 1478−1488.
(13) Nuss, M. C.; Planken, P. C. M.; Brener, I.; Roskos, H. G.; Luo, M. S. C.; Chuang, S. L. *Appl. Phys. B* **1994**, *58*, 249−259.
(14) Groot, M.-L.; Vos, M. H.; Schlichting, I.; Martin, J.-L. *Springer Ser. Chem. Phys.* **2001**, *66*, 686−688.
(15) Beard, M. C.; Turner, C. M.; Schmuttenmaer, C. A. *J. Am. Chem. Soc.* **2000**, *122*, 11541−11542.
(16) Kaplan, A. E. *J. Opt. Soc. Am. B* **1998**, *15*, 951−956.
(17) Ruffin, A. B.; Rudd, J. V.; Whitaker, J. F.; Feng, S.; Winful, H. G. *Phys. Rev. Lett.* **1999**, *83*, 3410−3413.
(18) McGowan, R. W.; Cheville, R. A.; Grischkowsky, D. *Appl. Phys. Lett.* **2000**, *76*, 670−672.
(19) Xu, J. Z.; Wang, L.; Yang, G. Z. *Chin. Phys. Lett.* **2000**, *17*, 568−570.
(20) Butcher, P. N.; Cotter, D. *The Elements of Nonlinear Optics*; Cambridge University Press: Cambridge, 1990.
(21) Cook, D. J.; Chen, J. X.; Morlino, E. A.; Hochstrasser, R. M. *Chem. Phys. Lett.* **1999**, *309*, 221−228.
(22) Atkins, P. *Physical Chemistry*, 6th ed.; W. H. Freeman: New York, 1997.
(23) Nuss, M. C.; Orenstein, J. In *Millimeter and Submillimeter Wave Spectroscopy of Solids*; Grüner, G., Ed.; Springer-Verlag: Berlin, 1998; Vol. 74, pp 7−50.
(24) Beard, M. C.; Schmuttenmaer, C. A. *J. Chem. Phys.* **2001**, *114*, 2903−2909.
(25) Bakker, H. J.; Cho, G. C.; Kurz, H.; Wu, Q.; Zhang, X. C. *J. Opt. Soc. Am. B* **1998**, *15*, 1795−1801.
(26) Castner, E. W.; Maroncelli, M. *J. Mol. Liq.* **1998**, *77*, 1−36.
(27) Kindt, J. T.; Schmuttenmaer, C. A. *J. Chem. Phys.* **1997**, *106*, 4389−4400.